10132 *Macromolecules* **2010**, *43*, 10132–10142
DOI: 10.1021/ma100490c

Macromolecules
ARTICLE

Impact of Polymer Molecular Weight on the Dynamics of Poly(dimethylsiloxane)−Polysilicate Nanocomposites

Glenn V. Gordon,[†] Randall G. Schmidt,*[,†] Marlitt Quintero,[‡] Natalie J. Benton,[‡] Terence Cosgrove,[‡] Val J. Krukonis,[§] Kara Williams,[§] and Paula M. Wetmore[§]

[†]*Dow Corning Corporation, Midland, Michigan 48686-0994, United States,* [‡]*School of Chemistry, University of Bristol, Cantock's Close, Bristol, BS8 1TS U.K., and* [§]*Phasex Corporation, Lawrence, Massachusetts 01843, United States*

Received March 3, 2010; Revised Manuscript Received October 7, 2010

ABSTRACT: Introducing hard spherical polysilicate nanoparticles up to 0.30 volume fraction into narrow molecular weight (M) fractions of poly(dimethylsiloxane) (PDMS) that spanned its unentangled and entangled polymer chain regimes produced transparent and colorless polymer nanocomposites (PNCs) with zero-shear-rate viscosities η_0 either greater or less than the polymer matrix. Below the PDMS critical molecular weight for chain entanglements to start influencing η_0 (M_c), nanoparticle inclusion increased the PNC η_0 consistent with the reinforcement mechanism from traditional fillers of much larger particle sizes. Conversely, PNCs using entangled PDMS ($M > M_c$) exhibited a reduction in η_0 within a certain concentration range of nanoparticles. The reduction in η_0 was proposed to be primarily due to the dilution of the entanglement density of polymer chains as evidenced by a shift to higher M_c that was a function of the volume fraction of polymer chains, ${\phi_1}^{-0.56}$, and an increase in the translational motion manifested through an increase in the polymer self-diffusion coefficient. In contrast to the ${\phi_1}^{-1}$ dependence of M_c in concentrated polymer solutions, the dilution effect of the polysilicate nanoparticle on the polymer chain entanglement density was moderated by polymer adsorption, hydrodynamic effects and to some extent by free volume. Above M_c, the PNC η_0 scaled as $\phi^2{\overline{M}_w}^{3.5}$ where $\overline{M}_w$ is the polymer weight-average molecular weight. Nuclear magnetic resonance T_2 spin−spin relaxation measurements found that the increase in polymer mobility due to the nanoparticles became evident only above $2M_c$. In contrast to the η_0 results, the transition to a stronger $\overline{M}_w$ dependence by $1/T_2$ shifted to lower M with increasing nanoparticle concentration.

Introduction

Particulate fillers are generally added to synthetic polymers to provide mechanical reinforcement and achieve specific performance criteria. However, this composite approach is typically accompanied by an increase in the zero-shear-rate viscosity η_0 that, in most instances, is undesirable with respect to processing and dispensing operations. The average particle size of traditional fillers such as calcium carbonate, carbon black, silica, and titanium dioxide ranges from 10 nm to 10^2 μm with many of the most commonly used reinforcing fillers residing in the upper range. The viscous effect of particulate fillers has been adequately described in the terms of volume fraction ϕ_2, maximum packing efficiency ϕ_m, and interaction (slip) at the particle−polymer interface.[1] In addition, the shape[1] and size distribution[2−4] of the particulates will influence the resulting composite η_0. Conversely, plasticizers are added to polymers to lower their glass transition temperature T_g thereby enhancing its molecular mobility and reducing η_0 over a specific temperature range of interest.[3]

Recent work[6−18] on polymer−nanocomposites (PNCs) based on nanoscale particles (1−100 nm) showed considerably different and often more complex behaviors. An apparent lack of universal trends in extending rheological reinforcement mechanisms of composites based on micrometer-sized colloidal fillers to nanosized fillers was often attributed to larger surface areas available for polymer−filler interactions when the particles are well dispersed and less than 100 nm in diameter.[19] Such complex behaviors were exemplified by the nonmonotonic response of a homogeneous system of polystyrene (PS) nanoparticles in linear entangled PS where viscosity increased at low nanoparticle concentrations followed by a reduction (relative to the polymer matrix viscosity) at higher concentrations that was found, in part, to depend on the presence or absence of chain polymer entanglements.[13,14]

Previous studies[7−12] addressed similar complexities in property trends using nuclear magnetic resonance (NMR) spin−spin relaxation and self-diffusion techniques and steady-shear viscosity measurements to probe the impact of trimethylsilyl-treated (weakly interacting) polysilicate nanoparticles on the dynamics of poly(dimethylsiloxane) (PDMS) polymers in different time scales. For polymers below M_c, the critical molecular weight for chain entanglements to start influencing η_0, a multiple exponential spin−spin relaxation response (T_2) was associated with three different types of polymer segmental mobility that became increasingly restricted with increasing nanoparticle concentration: (1) free, unperturbed chains; (2) perturbed polymer ascribed to loops and tails; (3) a highly constrained population of trains in direct contact with the nanoparticle surface. Therefore, the reinforcement mechanism from the inclusion of nanoparticles is being referred here in terms of restricted polymer mobility as manifested by shorter T_2 and, on a longer time scale, by an increase in the PNC $\eta_0(\phi_1)$ relative to polymer component viscosity $\eta_0(1)$, where ϕ_1 is the polymer volume fraction.

For polymers above M_c, the spin−spin relaxation and viscosity results were more complicated. Reinforcement was only observed above a critical nanoparticle concentration. Below this threshold,

*Corresponding author. E-mail: r.g.schmidt@dowcorning.com.

 Published on Web 11/02/2010

which appeared to depend on both the molecular weight M of the polymer and polysilicate as well as temperature T, the enhanced mobility (longer T_2) and reduced $\eta_0(\phi)$ were hypothesized to be a combination of free volume, polymer adsorption, and chain entanglement effects.[8] Molecular dynamics (MD) simulations and theoretical treatments have attempted to rationalize both viscosity-reinforcement and viscosity-reduction mechanisms of PNCs where, aside from ϕ_2, the nature of nanoparticle−polymer interactions, interparticle distance $2h$, and the ratio of particle (hydrodynamic) radius R to polymer radius of gyration R_g were cited.[20−25]

Understanding the impact of polymer size on the dynamics of PNCs can start from the power-law relationship between M and η_0 for both melts and concentrated solutions of linear polymers such as PDMS which, in turn, can be divided into unentangled, entangled, and pure reptation regimes, respectively

$$\eta_0 \sim M^1 \quad M < M_c \tag{1}$$

$$\eta_0 \sim M^\alpha \quad M_r > M > M_c \tag{2}$$

$$\eta_0 \sim M^3 \quad M > M_r \tag{3}$$

where M_r is the reptation molecular weight.[26] To accommodate a distribution of molecular weights, M is taken as the weight-average molecular weight $\overline{M}_w$. Historically, M_c was approximated to be twice the molecular weight between entanglements M_e although the ratio M_c/M_e was reported to vary with polymer chemical structure.[26] M_c marks the transition in the $\eta_0 \sim M$ relationship from that modeled by Rouse[27] and Bueche[28] described by eq 1 to the empirical relationship by eq 2 where the scaling exponent α has an experimentally recorded range of 3.5 ± 0.2 due to the effect of chain entanglements or topological constraints. The Doi−Edwards tube theory[29] based solely on the reptation relaxation mechanism proposed by de Gennes[30] predicts the relationship in eq 3 for the regime $M > M_c$ but this behavior was experimentally observed only at very high polymer molecular weights ($M/M_e \geq 10^2$) with the transition to this behavior occurring at M_r.[26,31,32] To explain the discrepancy in the scaling exponent, modifications to the Doi−Edwards theory were proposed in terms of contour length fluctuations[33,34] and constraint release.[35]

A single-exponential transverse spin−spin relaxation function was calculated[36−38] using the Rouse model to describe polymer chain dynamics in the regime $M < M_c$, where the relaxation rate can be expressed as

$$1/T_2 \sim \beta \ln M \quad M < M_c \tag{4}$$

where β is a fitting parameter with a dimension of reciprocal time. For sharp fractions ($\overline{M}_w/\overline{M}_n \leq 1.05$, where $\overline{M}_n$ is the number-average molecular weight) of linear PDMS at 293 K, β was reported to be 0.90 ± 0.03 s^{-1}.[39] At high M, a shift to a much stronger dependence of $1/T_2$ on ln M ($\beta = 14.7 \pm 0.9$ s^{-1}) occurred at 29.6 ± 1.5 kg·mol^{-1} reminiscent of the reported viscometric transition at $M_c = 29$ kg·mol^{-1} from a compilation of η_0 and $\overline{M}_w$ data for PDMS at 298 K.[40] However, the T_2 behavior above M_c was more complex and a nonexponential function with longer relaxations rates was expected and experimentally confirmed for PDMS.[39] The nonexponential relaxation, which increased with M, was attributed to a distribution of mobilities related to the proximity of the entanglement points and a greater mobility associated with chain ends.

In this paper, a more extensive series of narrow molecular-weight PDMS fractions spanning the unentangled and entangled regimes were blended with an amorphous trimethylsilyl-treated polysilicate to more adequately evaluate the effect of polymer molecular weight on the dynamics of PNCs. The spherical shape and size of this polysilicate nanoparticle ($R = 2 \pm 0.4$ nm) are more comparable to the polyhedral oligomeric silsesquioxanes (POSS) generating significant attention with respect to molecular reinforcement of polymeric materials for nanotechnologies.[18,41] Polysilicate materials have long been used to tune the viscoelasticity and enhance the durability of linear siloxanes in various commercial applications including pressure-sensitive adhesives and release linears.[42,43]

Experimental Section

Materials. The primary material set of entangled trimethylsiloxy-end blocked PDMS narrow molecular-weight fractions was derived from a Dow Corning 12,500 cSt 200 Fluid (lot 1812258) using supercritical fluid (SCF) extraction at Phasex Corporation (Lawrence, MA). A secondary set of narrow fractions and polydisperse polymers was assembled from previous studies and from in-house stock including Dow Corning 200 and UHV Fluids.

The trimethylsilylated polysilicate was supplied by Dow Corning Corporation, and designated here as R2 representing an intermediate particle size between two polysilicates from previous investigations.[7−12] It was synthesized via an acid-catalyzed polymerization of sodium silicate followed by a reaction with trimethylchlorosilane in a process described elsewhere[44] and using an equivalent molar ratio of trimethylsiloxy and silicate units to produce an amorphous powdery material with a T_g of 369 ± 3 K as determined by dynamic mechanical thermal analysis.

For each PNC series, the components were dissolved in reagent-grade xylenes to assist with dispersion of the polysilicate at specific volumetric ratios and mixed overnight on a tumbling device. To remove the solvent, the blends were exposed as thin films in a forced-air oven at 393 K for 16 h followed by 16 h under full vacuum at 343 K. The resulting solvent-free PNCs were clear and colorless, and measurements were conducted at least one month after preparation. Following the convention for composites,[1] the subscripts 1 and 2 denote the polymer and nanoparticle components, respectively.

Characterization. *Supercritical Fluid Extraction*. The general equipment and methodology for carrying out SCF extraction were explained in detail elsewhere.[45] 0.465 kg of a 12,500 cSt 200 Fluid was charged into an extraction vessel containing stainless steel mesh (Goodloe) area-enhancing packing with the vessel attached to the supercritical fluid extraction system. Carbon dioxide gas was compressed to a desired pressure (24−45 MPa) at 373 K and passed through the polymer charge. During contact between gas and polymer, the gas extracted those chains of molecular weight that dissolved in the gas at the particular combination of pressure and temperature. Downstream of the vessel the pressure was lowered to ambient (via a pressure reduction valve), and the extracted fraction was precipitated in a collector positioned at the outlet of the valve. By sequentially increasing the CO_2 pressure and collecting the soluble polymer fraction, nine narrow molecular weight fractions were collected totaling 0.450 kg (97% yield). The fractionation process is termed isothermal pressure profiling.

Size Exclusion Chromatography. The molecular weight properties of PDMS polymers were analyzed by size exclusion chromatography (SEC) instrumentation that consisted of a Waters 515 pump, 717 autosampler, and 2410 differential refractometer. The separation was made with two (300 mm × 7.5 mm) Polymer Laboratories PLgel 5-μm Mixed-C columns (separation range of 0.20 to 2,000 kg·mol^{-1}), preceded by a PLgel 5-μm guard column (50 mm × 7.5 mm). HPLC-grade toluene flowing at 1.0 mL·min^{-1} was the eluant with the columns and detector at 318 K. Solutions in toluene were prepared at 0.5% w/v polymer and filtered through a 0.45-μm PTFE syringe filter into glass autosampler vials. A 50-μL injection volume was used and data

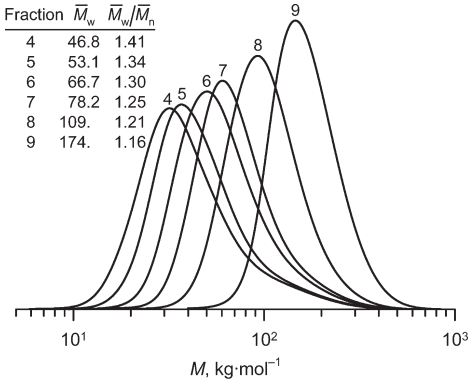

Figure 1. Molecular weight profiles of PDMS fractions obtained via SCF extraction of a Dow Corning 12 500 cSt 200 Fluid used in this study.

were collected for 25 min and processed using PE Nelson Access*SEC software. Molecular weight averages were determined relative to a third-order polynomial calibration curve derived from PS calibration standards covering a molecular weight range of 0.58−1,290 kg·mol^{-1}. Figure 1 shows the SEC profiles of the higher molecular weight PDMS SCF fractions obtained from the starting polymer, which was measured to have a $\overline{M}_w$ of 77.3 kg·mol^{-1} and a polydispersity $\overline{M}_w/\overline{M}_n$ of 2.76.

The $\overline{M}_w$ of some SCF extraction fractions was verified by light scattering using a Viscotek T-300 Triple Detector Array along with PLgel Mixed-D, Mixed-E and guard columns at 308 K, and HPLC-grade ethyl acetate as the eluant. An ASTM-certified PS ($\overline{M}_w$ = 94.637 kg·mol^{-1}) was used for instrument calibration. Values of 71.4, 109, and 176 kg·mol^{-1} were obtained for the three highest molecular weight fractions (78K, 109K, and 174K in Table 1) in good agreement with those recorded using the PS-calibrated SEC columns. Light-scattering signals from the lower molecular weight fractions were poorly resolved, and no comparisons were attempted. To avoid systematic errors, only M values based on the PS calibration standards were considered for this paper (Table 1).

The molecular weight properties of the polysilicate were determined using a SEC set up that included a Waters 2695 Separation Module equipped with two (300 mm × 75 mm) Polymer Laboratories Mixed-D columns (linear separation range of 0.2 to 400 kg·mol^{-1}) calibrated with SCF-derived polysilicate molecular weight fractions, a Miran1A-CVF HPLC infrared detector (9.1 μm; 1099 cm^{-1} Si−O−Si), and HPLC-grade chloroform as the eluant at 308 K (Table 1).

The molecular size and shape of the R2 nanoparticle at 298 K were characterized by small-angle neutron scattering (SANS) in a concentration series of the polysilicate (scattering length density of 0.89 × 10^{-4} nm^{-2}) in toluene-d.[12] SANS measurements were conducted using the LOQ instrument (neutron wavelengths λ between 0.22 and 1.0 nm; scattering vector Q range of 0.07−2.49 nm^{-1}) at ISIS (U.K.) and the D11 instrument (λ = 0.46 nm; Q range of 0.04−5.1 nm^{-1}) at ILL (France). Using the Guinier approximation in the range of 0.07 nm^{-2} > Q^2 > 0.5 nm^{-2}, the average value for the R_g was 1.5 ± 0.3 nm. The SANS data were successfully fitted to a hard-sphere model to validate a predominantly spherical shape of the polysilicate molecules. An extensive analysis of the size and shape of polysilicate particles using SANS is provided elsewhere.[13]

Density. Polymer density was measured at 293 K using an Anton PAAR DMA48 density meter with a specified accuracy and precision of 1 × 10^{-1} and 3 × 10^{-2} kg·m^{-3}, respectively. For the polysilicate, a concentration series of solutions in tetrahydrofuran was prepared up to 20 wt % in order to extrapolate a density of 1137 kg·m^{-3} following a procedure described elsewhere,[48] which was in good agreement with that found by helium pycnometry (1139 kg·m^{-3}) using a Quantachrome Micropycnometer MPY-2 with PM Task 80773 spheres as calibration standards.

Rheology. Steady-shear viscosity was characterized as a function of shear rate to determine η_0 at different temperatures using TA Instruments RDA-type rheometers equipped with spring transducers that provided a torque range of 0.02−200 mN·m, a forced-convection oven, and 25- or 50 mm-diameter cone-and-plate fixtures with nominal cone angles of 0.10 and 0.04 radians, respectively. The gap between fixtures was zeroed at each temperature to maintain the manufacturer-specified truncation. The Newtonian region of all the polymers and PNCs was within the accessible shear-rate range of the rheometers. The results for η_0 at 298 and 353 K are summarized in Table 1. Newtonian behavior was observed for all of the PNCs over the entire shear rate range consistent with a system that is devoid of particle agglomeration.

Nuclear Magnetic Resonance. ^{1}H spin−spin relaxation measurements were performed using a Carr−Purcell−Meiboom−Gill (CPMG)[49,50] pulse sequence with a 180° pulse separation of 2.5 ms. Up to 2048 data points were collected by sampling alternate echo maxima. Measurements were carried out at two temperatures on a Bruker Avance 400 NMR spectrometer operating at 400 MHz for protons. The temperature of the sample was controlled by an airflow system with an accuracy of ±0.3 K.

For high M polymers especially with added fillers, local chain motion will be constrained and in many cases, anisotropic. If motion is so restricted that the sample is effectively a solid, the spin−echoes in the CPMG sequence will not detect these and the initial heights of the extrapolated decays will be less than that expected if all the protons were visible. As ϕ_2 increases not only is the signal less per unit volume as the nanoparticles take up space in the PNC but an increasing fraction of polymer segments will become immobilized. For this reason the data were normalized to unity such that the shapes of the decays can be compared.

Given that the PNCs not only contained polymer segments in a variety of environments but also that these individual relaxation components may not be exponential, a representative T_2 parameter was used as a phenomenological approach for providing an effective comparison with η_0 data. The approach used here was to fit the data using a multiple-exponential fitting (DISCRETE) algorithm[51] to provide an averaged relaxation time parameter. The data were fitted with up to n distinct exponentials in the form

$$I(t) = \sum_{i=1}^{n} I_i^0 \exp(-t/T_{2,i}) + b \tag{5}$$

where I_i^0 is the protonic proportion of component i with relaxation $T_{2,i}$ and b the baseline, which should be zero except for any DC offsets. The choice of best fit was based on a nonlinear correction to the standard deviation of the fit to the data for different integers of n. A weighted average T_2 was calculated taking into account the relative proportions of each exponential component.

Polymer self-diffusion measurements were conducted using the pulsed-gradient spin−echo (PGSE) NMR technique. Test specimens were placed in 5 mm NMR tubes no more than 10 mm in depth. The results were analyzed by nonlinear least-squares fits to the equation for unrestricted diffusion

$$\frac{I(\delta,\Delta,g,\tau)}{I_0} = \exp(-2\tau/T_2)\exp[-\gamma^2 g^2 \delta^2 (\Delta - \delta/3) D_s] + b \tag{6}$$

where I_0 is the initial spin−echo signal intensity at τ = 0 in the absence of any gradient, τ the time (100 ms) between the 90° and 180° pulses, γ the gyromagnetic ratio, g the magnitude of the field gradient pulse, Δ the distance between the leading edges of the gradient pulses (100 ms), δ the length of the gradient pulse, and D_s the self-diffusion coefficient. Data for the PNCs were fit to the single diffusive process described by eq 6.

Table 1. Physical Properties of PDMS and Polysilicate Components

material	$\overline{M}_w$[a] (kg·mol^{-1})	$\overline{M}_w/\overline{M}_n$	R_g[b] (nm)	ρ(293 K)[c] (kg·m^{-3})	η_0 (Pa·s) 298 K	η_0 (Pa·s) 353 K
			PDMS Narrow Fractions			
1K[d]	1.3	1.02	0.96	945	0.0094	–
6K	6.0	1.08	2.05	963	0.046	0.018
12K	12.2	1.03	2.93	970	0.119	0.048
13K	13.0	1.07	3.02	971	0.142	0.058
31K	31.4	1.10	4.70	974	0.837	0.345
47K	46.8	1.41	5.74	975	2.45	0.970
53K	53.1	1.34	6.11	975	3.69	1.44
67K	66.7	1.30	6.85	975	7.44	2.93
78K	78.2	1.25	7.42	976	12.8	5.02
109K	109.	1.21	8.76	976	42.9	16.9
174K	174.	1.16	11.1	977	254.	99.9
793K	793.	1.17	23.6	*978*	55800.	21600.
904K	904.	1.19	25.2	*978*	91000.	46600.
			Polydisperse PDMS			
5K*p*	4.6	1.32	1.80	*963*	0.036	0.014
21K*p*	21.5	1.68	3.89	*971*	0.355	0.132
36K*p*	36.1	1.68	5.04	*972*	1.31	0.486
37K*p*	36.9	1.56	5.09	*972*	1.46	0.540
117K*p*	117.	2.37	9.06	*976*	64.5	25.3
139K*p*	139.	1.53	9.89	*977*	128	49.4
143K*p*	143.	2.00	10.0	*977*	122.	45.1
179K*p*	179.	2.17	11.2	*977*	323.	122.
216K*p*	216.	2.14	12.3	*978*	715.	272.
			Polysilicate			
R2	5.6	2.0	1.5	1137		

[a] Based on PS- and polysilicate-calibrated SEC columns for PDMS and R2, respectively. [b] Calculated for PDMS from the relationship $0.839\overline{M}_w^{0.5}$ at 298 K.[46] [c] Italicized density values based on historical data for commercial-grade PDMS. [d] Reference 47.

A solid-state spectrum was obtained at 298 K to estimate T_2 for the polysilicate because of the strong dipolar coupling found in solids. A single 90° pulse experiment was conducted on a Bruker Avance spectrometer operating at 300 MHz for protons with the test specimen placed in a 7 mm zirconia rotor. The resultant spectrum was fitted to a sum of a Gaussian and a Lorentzian function. The full-width at half-height $\Delta\nu$ was $1.67/\pi T_2$ and $1/\pi T_2$ for the Gaussian and Lorentzian functions, respectively. The weighted-average T_2 for R2 was 36 μs.

Results and Discussion

The presentation and discussion of the results from viscosity and NMR measurements are organized as follows: First, the physical mechanisms for the $\eta_0 \sim \overline{M}_w$ relationship for PDMS are revisited for the different M regimes using data collected at 298 and 353 K. Next, the pure polymer data are compared with results from the PNCs at two different nanoparticle concentrations. The impact of the polysilicate nanoparticle on PDMS viscosity is discussed for three molecular weight regimes: (1) $M < M_c$; (2) $M \sim M_c$; (3) $M > M_c$. Finally, the viscosity data are compared with the NMR spin−spin relaxation results.

The PNCs were prepared at 17 and 30 vol % particle loadings. The loadings were chosen to produce viscosity changes from the pure melt that can be readily differentiated using a standard laboratory rheometer and where the outcome can be potentially meaningful for product systems that employ these components. However, the high particle loadings do increase the potential for particle aggregation in the PNC which could complicate the results. Although recognizing to the possibility that some aggregation can occur, several published behaviors of this PNC system suggest that particle aggregation was not appreciable, namely: (1) SANS experiments revealed the polysilicate nanoparticles to be successfully dispersed with a stabilizing layer of PDMS when analyzed as a solution in toluene.[12] Adsorption by PDMS in the melt will prevent depletion flocculation and effectively stabilize the dispersion of the nanoparticles consistent with the shelf stability of this PNC system observed over 3 years at ambient conditions; (2) unlike silica fillers, the addition of polysilicate nanoparticles were found to progressively retard the crystallization of PDMS near −45 °C with no crystallization observed beyond 26 vol % particle loading suggesting that the particles dispersed and interacted with the polymer chains on a molecular level;[10] (3) optically clear blends over broad composition ranges are obtained, and the viscosity profiles are Newtonian over extended ranges of shear rate.[12,13]

Polymer Viscosity. Figure 2 plots η_0 for PDMS at 298 and 353 K as a function of $\overline{M}_w$ for both the narrow molecular weight fractions and polydisperse polymers combined; the data are also listed in Table 1. M_c occurred at approximately 28 kg·mol^{-1} based on the intersection of two power-law least-squares regression fits as it is generally accepted that the transition between the two M regimes is gradual rather than sharp. The power-law dependence of η_0 was $\overline{M}_w^{1.5}$ and $\overline{M}_w^{3.5}$ below and above M_c, respectively. These results were expectedly independent of temperature T and consistent with cited values at 298 K compiled from nine sources of published data by Friedman and Porter:[40] $M_c \sim 29$ kg·mol^{-1}; $\overline{M}_v^{1.48\pm0.02}$ for $M < M_c$; and, $\overline{M}_v^{3.6\pm0.2}$ for $M > M_c$, where $\overline{M}_v$ is the intrinsic-viscosity-average molecular weight.

For linear polymers in the regime $M < M_c$, deviation of experimental data from the Rouse prediction given by eq 1 was ascribed to the concentration effect of chain ends on free volume such that the observed power-law exponent ranges from 1 to 2.5. The difference can be accounted for by the monomeric friction coefficient ζ_0, which depends on the fractional free volume f, T, and M. Self-diffusion data from

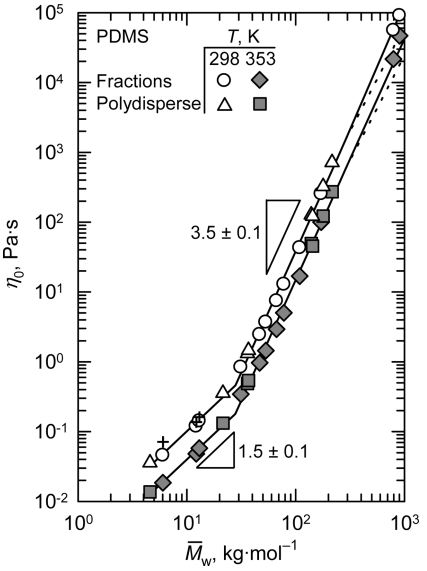

Figure 2. Molecular weight dependence of the zero-shear-rate viscosity of PDMS. For fractions with $\overline{M}_w < 29$ kg·mol^{-1}, η_0 corrected for the effect of chain ends (+) recovered the M^1 dependence. The dotted line refers to the predicted M^3 scaling relationship above M_r (290 kg·mol^{-1}).[26]

spin−echo NMR[12,52] and viscoelastic measurements[53] provided a $\zeta_0 \sim \overline{M}_n$ relationship for PDMS at 298 K. Noting that ζ_0 was not a simple function of $\overline{M}_n^{-1}$ over the entire range below M_c, interpolated coefficients of 5.8, 7.9, and 8.0 pN·s·m^{-1} were determined for the 6K, 12K, and 13K fractions, respectively. The M^1 dependence predicted by eq 1 was recovered by correcting the experimentally measured η_0 by the factor ζ_0^∞/ζ_0, where the limiting value at high M, $\zeta_0^\infty(M \geq M_c)$, was reported as 9 pN·s·m^{-1} for PDMS at 298 K.[53] The constant-friction $\eta_0\zeta_0^\infty/\zeta_0$ values for the PDMS fractions ($M < M_c$) at 298 K are represented by the + symbol in Figure 2.

Figure 2 also plots data from two high molecular weight polymers—793 and 904 kg·mol^{-1} —which were above the cited range of M_r for PDMS (290−430 kg·mol^{-1}).[26] Noting that $M/M_e < 10^2$ where $M_e = 9.6$ kg·mol^{-1},[53] the results were more aligned with the $M^{3.5}$ dependence (depicted by extended solid lines) rather than M^3 (dotted lines originating from $M_r = 290$ kg·mol^{-1}) based on a reptation and constraint release model.[35] This was consistent with previous observations that the condition $M/M_e \geq 10^2$ was necessary before the onset of the M^3 dependence becomes apparent.[26,31,32]

Polymer Nanocomposite Viscosity. Figure 3 shows the impact of incorporating the polysilicate nanoparticle at two concentrations on the $\eta_0 \sim \overline{M}_w$ relationship of PDMS fractions at 298 K (left) and 353 K (right). As ϕ_1 decreased from 1.0 to 0.70, the data listed in Table 2 suggested a shift in $M_c(\phi_1)$ to higher PDMS molecular weights from 27 kg·mol^{-1} to 33 kg·mol^{-1}, and a decrease in the power-law exponent describing the $\eta_0 \sim \overline{M}_w$ relationship both below and above $M_c(\phi_1)$. Taking into account experimental uncertainty, the results in both M regimes were also insensitive to T.

Figure 4 highlights contrasting effects on the PNC viscosity in the two M regimes delineated by $M_c(\phi_1)$, where $\eta_0(\phi_1)/\eta_0(1)$ is plotted as a function of ϕ_1 for several polymer fractions at 298 K (left) and 353 K (right). With respect to relative viscosity, the polysilicate nanoparticles were considered to reinforce the polymer matrix if $\eta_0(\phi_1)/\eta_0(1) > 1$ or to

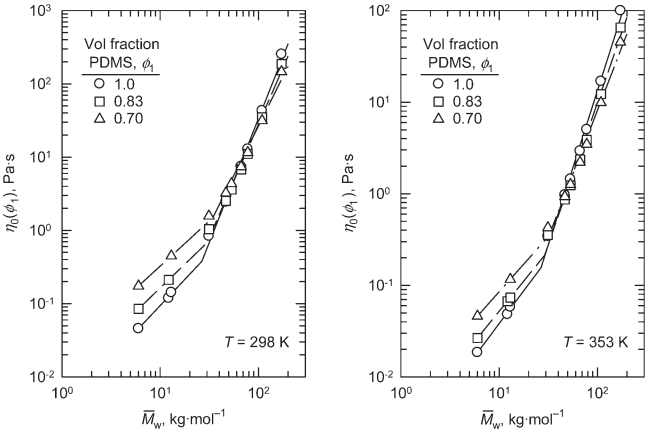

Figure 3. Effect of polysilicate nanoparticle concentration on the molecular weight dependence of the zero-shear-rate viscosity of PDMS at 298 K (left) and 353 K (right).

Table 2. Effect of Polysilicate Nanoparticle on the Molecular Weight Dependence of Viscosity of PDMS

		power-law exponent from $\eta_0 \sim \overline{M}_w$			
		$\overline{M}_w < M_c(\phi_1)$		$\overline{M}_w > M_c(\phi_1)$	
volume fraction PDMS, ϕ_1	$M_c(\phi_1)$, kg·mol^{-1}	298 K	353 K	298 K	353 K
1.0	27	1.43	1.43	3.38	3.36
0.83	30	1.30	1.32	3.09	3.10
0.70	33	1.23	1.21	2.70	2.78

plasticize PDMS if $\eta_0(\phi_1)/\eta_0(1) < 1$. Unlike results reported for a PNC system of PS nanoparticles in linear PS,[14,15] the apparent smooth trends referenced by only a triplet of data points for each polymer fraction are supported by earlier studies[7−9,12] utilizing a more extensive series of nanoparticle concentrations including that of a larger polysilicate (R3: $R = 1.7$ nm; $\overline{M}_w/\overline{M}_n = 3.0$) and over a wide range of PDMS molecular weights. Smooth transitions starting with an initial viscosity reduction prior to an eventual reinforcement were also found from two types of untethered POSS when either nanoparticle was blended with a poly(methyl methacrylate) (PMMA) although the latter mechanism was complicated by the presence of POSS crystallites.[18]

Impact of the Polysilicate Nanoparticles on PDMS below M_c. Polymer reinforcement as manifested by $\eta_0(\phi_1)/\eta_0(1) > 1$ was observed at both nanoparticle concentrations if $\overline{M}_w < M_c$ for PDMS (Figure 4). This followed reported results using the R3 polysilicate.[7,8] Reinforcement was also evident for the 31K polymer, which was just above M_c, in concert with data using the R3 polysilicate[9] and these results are addressed in the next section.

For $\overline{M}_w < M_c$, $\eta_0(\phi_1)/\eta_0(1)$ exhibited a quadratic increase with ϕ_2 in accordance with the predicted effect from hydrodynamic interactions and Brownian forces. Figure 5 plots a more extensive concentration series using the 6K fraction at 298 K, which for PDMS is less than M_e (9.6 kg·mol^{-1}).[46] In the limit of $\phi_2 < 0.1$, the relative viscosity data represented by the circle symbol were consistent with the quadratic equation derived by Batchelor[54]

$$\frac{\eta_0(\phi_1)}{\eta_0(1)} = 1 + (5/2)\phi_2 + 6.2{\phi_2}^2 \qquad (7)$$

where 5/2 is the Einstein coefficient.[55,56] For $\phi_2 < 0.3$, an adequate fit was provided by the empirical eq 8 proposed

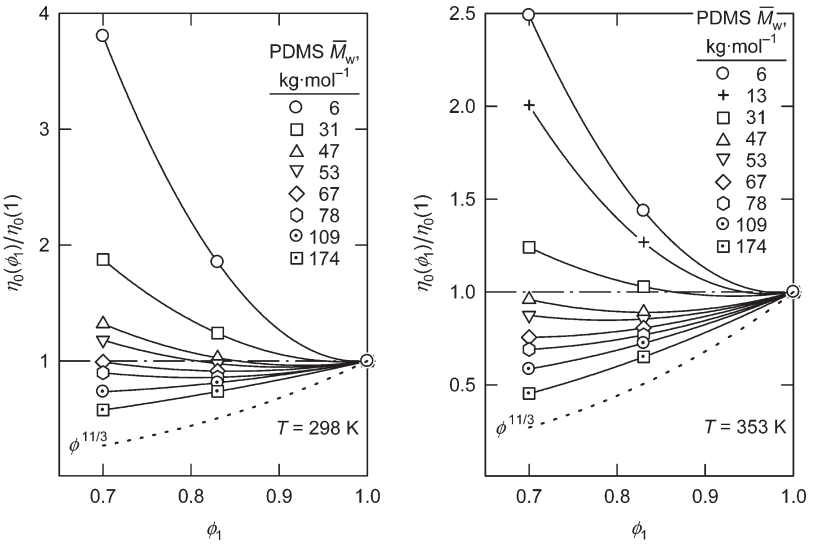

Figure 4. Nanocomposite viscosity relative to the PDMS polymer component at 298 K (left) and 353 K (right) as a function of the polymer concentration and weight-average molecular weight.

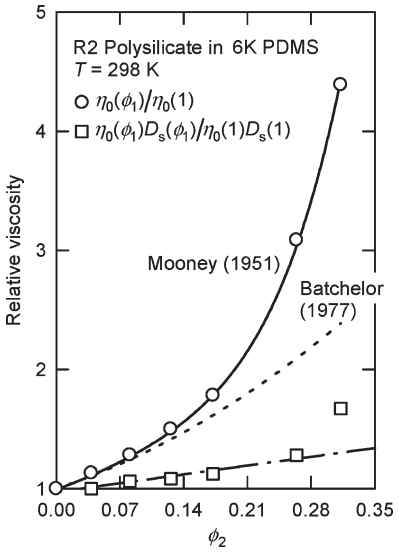

Figure 5. Effect of polysilicate concentration on the relative viscosity of a 6K PDMS fraction at 298 K and when viscosity is adjusted for the change in the self-diffusion of the polymer chains.

by Mooney[57] using the confirmation from SANS experiments[12] that the R2 polysilicate nanoparticles were well dispersed hard spheres such that the Einstein coefficient of 5/2 applied.

$$\ln \frac{\eta_0(\phi_1)}{\eta_0(1)} = \frac{(5/2)\phi_2}{1-\phi_2/\phi_m} \tag{8}$$

where ϕ_m is the only fitting parameter for the system under consideration here. Noting the sensitivity of $\eta_0(\phi_1)$ at high particle concentrations,[58] $\phi_m = 0.66 \pm 0.02$ ($\phi_2 = 0.3$) was experimentally determined which is consistent with the dense random close packing of spheres ($\phi_m = 0.64$). Hence, these results were further evidence that for polymers below M_c, the polysilicate nanoparticle functioned as a typical reinforcing filler for a PDMS matrix.

In the regime $M < M_c$, the experimental $\eta_0 \sim \overline{M}_w$ power-law exponent decreased from 1.4 to 1.2 with increasing nanoparticle concentration (Table 2) approaching the M^1 Rouse dependence. Geometric space-filling considerations point to the likelihood that the polysilicate nanoparticle reduced the polymer free volume in addition to the following arguments: (1) free volume scales with specific volume and the nanoparticle has a higher density than PDMS, and (2) a shift in the calorimetric T_g of PDMS to higher temperatures has been reported for polysilicates.[10,12] Tuteja et al.[15] also explained a viscosity increase on both these factors for homogeneous blends of PS nanoparticles in unentangled linear PS.

PGSE−NMR Diffusion Measurements. The viscosity increase due to the nanoparticles can also be in part attributed to enhanced frictional resistance. For the R2/6K system in Figure 5, attenuation decays from PGSE−NMR diffusion measurements[12] were fitted to the single-component diffusion equation given by eq 6 for which $D_s = 9.7\ (\pm 0.1) \times 10^{-12}\ m^2 \cdot s^{-1}$ was calculated for the 6K polymer. Single-diffusion fits were also adequate for the PNCs as the polysilicate at 298 K was invisible on the NMR time scale because of a short T_2 (weighted average of 36 μs) and the local mobility of the polymer chains as viewed by T_2 was primarily associated with segmental motion which has a much shorter correlation time than any motion of the particle. To assess the validity of this approach the diffusion coefficient of the particles was estimated from the Stokes−Einstein relation to be $D_s = 2.5 \times 10^{-12}\ m^2 \cdot s^{-1}$ (using a melt viscosity of 0.045 Pa·s for the 6K polymer). Given that the particle is likely to be partially adsorbed with the polymer suggests that the value of the particle diffusion coefficient here is an overestimate and as a first approximation can be considered independent of polymer diffusion. Hence, D_s values reported here represent polymer diffusing among chains and nanoparticles.

The PNCs exhibited a linearly increasing baseline PGSE signal with increasing ϕ_2, which should reflect the proportion of protons from mobile polymer segments but with increasingly restricted translational motion (long T_2). Candidates for this population of polymer segments would primarily be loops and tails—from polymer chains adsorbed onto nanoparticle surfaces—which possess high local mobility due to flexibility of the siloxane backbone, and a smaller proportion which would be entangled for sufficiently long times (~100 ms)

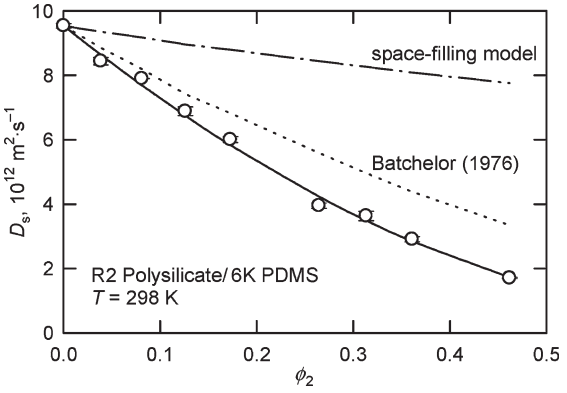

Figure 6. Effect of polysilicate concentration on the self-diffusion of a 6K PDMS fraction at 298 K.

with the adsorbed layer. Figure 6 plots $D_s(\phi_2)$ using the unentangled 6K polymer at 298 K, which revealed up to a 5-fold decrease in translational motion for the time scale of the PGSE−NMR experiment. An analogous form to eq 8 was used to empirically fit the D_s data.

If the nanoparticles merely acted as obstacles to diffusion, the change in D_s should be described by a simple space-filling restriction model such as

$$\frac{D_s(\phi_1)}{D_s(1)} = \frac{1}{1+\phi_2/2} \tag{9}$$

At a constant D_s, the difference between the calculated values from eq 9 and experimental data can be used to estimate the volume fraction of nanoparticles with an adsorbed polymer layer; that is, the actual volume fraction acting as barriers to diffusion will always be greater than the nanoparticle concentration.

The absence of hydrodynamic information factors into the difference between the data and eq 9 depicted in Figure 6. Within this ϕ_2 range, the interparticle separation $2h$ will decrease by approximately ${\phi_2}^{-1}$. Assuming no polymer adsorption onto the particle surface and that the polymer chain dynamics are not significantly altered, friction will become significant once $h < R_g$ of the polymer. Above the Einstein concentration limit, interparticle effects will contribute to the dynamics of the polymer and this contribution increases as ϕ_2 increases thereby requiring a more complex treatment to account for hydrodynamic interactions.

The model proposed by Batchelor[59] for the Brownian diffusion of rigid spheres when interparticle and hydrodynamic interactions were considered is given by

$$\frac{D_s(\phi_1)}{D_s(1)} = 1 - 1.83\phi_2 + 0.91{\phi_2}^2 \tag{10}$$

This hydrodynamic model, assuming that the polymer coils can be treated as effective hard spheres with hydrodynamic interactions, is shown as the dotted curve in Figure 6. The effect of including interactions, significantly reduced the discrepancy with the experimental data, but indicated that polymer chains still diffused more slowly at all nanoparticle concentrations. An adsorbed polymer layer could account for this difference, which would increase with increasing nanoparticle concentration thereby lending support to the hypothesis for an increasing proportion of polymer chains involved in a boundary layer.

The role of friction on the PNC viscosity can be analyzed in terms of D_s. The result is included in Figure 5 where $\eta_0(\phi_1)/\eta_0(1)$ was corrected by the ratio $D_s(\phi_1)/D_s(1)$. For $\phi_1 > 0.7$, the correction reduced the viscosity increase to a linear dependence on particle concentration with an Einstein coefficient of 0.9 ± 0.2, which appeared to imply slip of polymer chains at the nanoparticle surface already "coated" with a layer of adsorbed polymer chains. The deviation at higher concentrations was assigned to the depletion of unperturbed polymer chains as evidenced from NMR relaxation data and higher order particle interactions.

Ganesan et al.[23] proposed a continuum model based on the Rouse model for the dynamics of nanoparticles in an unentangled polymer matrix based on situations where R for the spherical particles was larger than the polymer correlation length but comparable or smaller than the polymer R_g

$$\frac{\eta_0(\phi_1)}{\eta_0(1)} - 1 = \frac{3 - 96\lambda(R_g/R)^2}{2[1 + 5\lambda + 48\lambda(R_g/R)^2]}\phi_2 \tag{11}$$

where λ is a dimensionless slip length ($\lambda \rightarrow 0$ for no slip and $\lambda \rightarrow \infty$ for perfect slip). If $R_g/R \gg 1$, the relative viscosity will scale as $-\phi_2$ such that $\eta_0(\phi_1) < \eta_0(1)$.

For the system in Figure 5, $R_g/R \sim 1$ and $\eta_0(\phi_1) > \eta_0(1)$ for all ϕ_1. Testing eq 11 experimentally will require R to approach the length scale of a PDMS monomer unit to satisfy the condition $R_g/R \gg 1$ given the upper boundary condition $R_g \leq 2.6$ nm for unentangled PDMS ($M_e = 9.6$ kg·mol^{-1}).[46] In an earlier paper,[10] a R1 silicate with $R = 0.45$ nm represented the lower size limit for this family of trimethylated silicates where T_g is a strong function of nanoparticle size. Its calorimetric T_g of 216 K was above that of the PDMS matrix (150 K), but below room temperature and was considered to be representative of a soft nanoparticle. The dilution of $\eta_0(1)$ by R1 for $\phi_1 > 0.7$ scaled with $-1.9(\pm 0.06)\phi_1$ for an unentangled PDMS ($M < M_e$; $R_g/R \sim 4.4$).

Impact of the Nanoparticle on M_c for PDMS. From Table 2, the shift to a higher onset of M_c for PDMS was quantified as a function of ϕ_1

$$M_c(\phi_1)/M_c = {\phi_1}^{-0.56} \tag{12}$$

As depicted in Figure 7, this scaling relationship with polymer volume fraction was less than the ${\phi_1}^{-1}$ dependence for a small molecule in a concentrated polymer solution that dilutes the polymer entanglement density.[60,61] This mechanism was previously assigned[62] to the reduction in the rubbery plateau modulus G_N^0 of a dimethylsiloxane-*co*-phenylmethylsiloxane copolymer, $\overline{M}_w = 600$ kg·mol^{-1}, by this type of polysilicate according to the relation $G_N^0(\phi_1)/G_N^0(1) = {\phi_1}^{2.6\pm0.3}$. Experimental values of the concentration exponent typically range from 2 to 2.3 for small molecule diluents.[63] The exponent is as follows: (1) 2 if, neglecting chain-end corrections, every contact between two chains has a constant probability of entanglement;[63] (2) $^7/_3$ for Θ solvents according to the argument that a fixed number of binary contacts constitutes an entanglement strand;[64,65] (3) $^9/_4$ from scaling laws applied to conditions for the overlap of random coils;[66] (4) 2.3 from a proposed unified phenomenological description that covered the melt, Θ-solution, and good-solvent regimes up to the overlap concentration.[67]

The shift in M_c to higher M has been inferred from earlier studies of similar siloxane PNCs,[7,9,12,62] but it was only in this present work that it was directly observed by using a more extensive M range. Given the observed scaling exponent for G_N^0, the corresponding exponent in eq 12 was expected to be $1-2.6 = -1.6$.[68] The weaker (−0.56) concentration dependence of M_c is proposed to be a combination

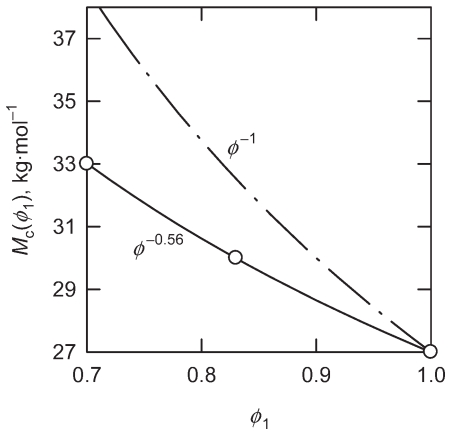

Figure 7. Effect of the polysilicate nanoparticle on M_c of PDMS.

of free-volume reduction and hydrodynamic interactions that perturbed the polymer chain dimensions such that the onset of entanglement effects was ultimately influenced by polymer adsorption onto the nanoparticle surface.

From Table 2, M_c for the PDMS fractions was found to be 27 kg·mol^{-1}, or 1 kg·mol^{-1} less than that found when including the more polydisperse polymers. In blends with the polysilicate, M_c shifted to 30 kg·mol^{-1} and 33 kg·mol^{-1} for ϕ_1 of 0.83 and 0.70, respectively. Given the uncertainty in calculating M_c, it was conceivable that the polysilicate-filled 31K polymer shown in Figure 4 was still in the Rouse−Bueche regime such that a reinforcement effect was observed at these concentrations.

Impact of the Polysilicate Nanoparticle above M_c for PDMS. Figures 3 and 4 provide evidence for the impact of the polysilicate on $\eta_0(1)$ in two polymer M regimes. Above M_c, a concentration boundary existed where $\eta_0(\phi_1)/\eta_0(1) < 1$. The results above M_c may be due to additional effects by the polysilicate on the chain dynamics of entangled polymers. The additional M dependence of $\eta_0(1)$ beyond pure reptation has been attributed to factors such as contour length fluctuations[33,34] and constraint release.[35] The nanoparticles may also be viewed as well dispersed "fixed" topological obstacles. The measured relaxation times of the particle protons are primarily due to intra particle dipolar interactions and the short T_2 (36 μs) is an indication of the rigidity of the nanoparticle. Therefore, the reduction in the $\eta_0 \sim \overline{M}_w$ power-law exponent from 3.4 to 2.7 (Table 2) may be an indication that the dynamics due to chain entanglements and constraint release were significantly impacted.

A maximum reduction in $\eta_0(\phi_1)/\eta_0(1)$ and subsequent crossover from plasticization to a reinforcement regime were both concentration and temperature dependent with both being delayed to higher ϕ_2 with increasing polymer M and increasing T. These results agreed with previous studies using both this spherical polysilicate[12]—where an Arrhenius-type activation energy of 4 kJ·mol^{-1} was found to describe the temperature dependence of the maximum reduction in η_0—as well as a larger ellipsoidal polysilicate[7,9] in a more extensive concentration series with entangled PDMS. In both instances, the nanoparticles were approximately equal or smaller in size R compared to the polymer R_g.

The viscosity reduction of PNCs through introduction of well-dispersed nanoparticles within a certain concentration regime has been described for a few other systems. Mackay et al.[14−16] reported that while polymer chain entanglement was a prerequisite, viscosity reduction was attributed to polymer confinement (when $R_g/h > 1$); when $R_g/h < 1$, as was the case for low ϕ_2, $\eta_0(\phi_1)/\eta_0(1) > 1$. It was proposed that incorporation of nanoparticles (1) induced a constraint release mechanism partly responsible for reducing η_0 without initially impacting G_N^0 and (2) introduced free volume at higher concentrations because of a large ratio between surface area and volume that would influence the entanglement density. Kopesky et al.[18] ascribed the phenomenon to an increase in free volume from nonreactive POSS nanoparticles well dispersed at low concentrations ($\phi_2 < 0.10$) in entangled PMMA. Marin et al.[69] used solutions of a 10K polybutadiene in a naphthenic hydrocarbon oil to demonstrate that a monotonic increase in viscosity was recovered when the blend viscosity was adjusted to the same free volume fraction as the undiluted sample.

Molecular simulations and theoretical treatments have also been applied to investigate the dynamics of chains and nanoparticles to elucidate the viscosity reduction mechanism. Kairn et al.[22] revealed that a small change in particle size impacts viscosity behavior: for a polymer matrix with an rms radius of gyration approximately twice that of the 0.78 nm particle radius in their simulation system, viscosity increased with particle concentration; however, when the particle radius was reduced by just over a factor of 2 such that it was roughly the size of a polymer monomer unit, the particle functioned as a solvent to dilute viscosity. Ganesan et al.[23] suggested that a higher proportion of their theoretical predictions would be valid for entangled polymers using the length scale d_t/R, where d_t is the reptation tube diameter. For weakly interacting nanoparticles in entangled polymers, which was the case here for the PDMS−polysilicate PNC system, viscosity reduction was predicted to be accentuated due to loss of entanglements. The effect of these length scales on viscosity reduction is addressed in the companion paper.[13]

Following scaling arguments[64,65] for entanglement lengths and assuming that the nanoparticles did not change the overall chain conformation, Ganesan et al.[23] suggested that

$$\frac{\eta_0(\phi_1)}{\eta_0(1)} = {\phi_1}^{11/3} \tag{13}$$

This prediction overestimates the viscosity reduction when compared to the data in Figure 4 where $d_t/R \sim 3$.

The PGSE−NMR diffusion measurements for these siloxane PNCs are to be reported in more detail elsewhere.[70] Figure 8a inset shows the effect of the nanoparticle concentration on D_s(298 K) in the regime $M_c < M \leq 109$ kg·mol^{-1}, which was significantly different from that observed in Figure 6 for an unentangled polymer. It should also be noted that D_s for the pure melt did not fit the reptation prediction of M^{-2}.

The PGSE−NMR results suggested that the translational motion of entangled polymer chains increased with incorporation of polysilicate nanoparticles. Figure 8 provides different pictures for the impact of the nanoparticles above M_c if this frictional effect was accounted for by D_s: (a) the reduction in relative viscosity was evident only at $\phi_1 = 0.83$ and only up to 67K although this does not preclude viscosity reduction for the higher M polymers occurring for $\phi_1 > 0.83$; (b) the molecular weight dependence of viscosity increased with nanoparticle concentration, where the power-law exponent increased from 3.4 for $\phi_1 = 1$ to 4.7 for $\phi_1 = 0.70$.

Tuteja et al.[15] reported that relative viscosity of linear PS did not scale with the volume fraction of PS nanoparticles which appeared to be consistent with the results depicted in Figures 3 and 4. However, based on the $M_c \sim \phi_1$ relationship described by eq 12, $\eta_0(\phi_1)/\eta_0(1)$ should scale with ϕ_1 and M within a certain concentration regime. Figure 9 shows the

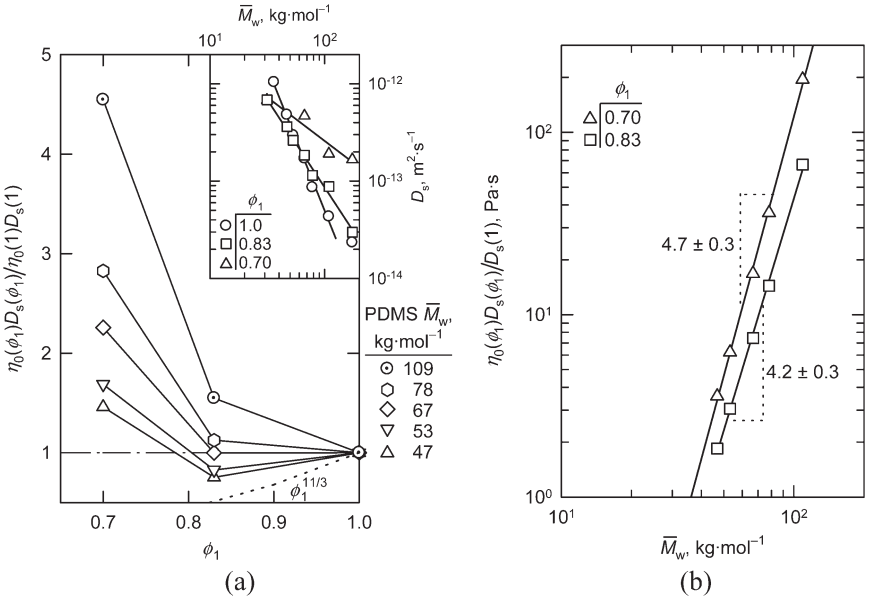

Figure 8. (a) Relative viscosity normalized by the self-diffusion coefficient as a function PDMS concentration and molecular weight at 298 K. Shown inset is the molecular weight dependence of the diffusion coefficient as a function of PDMS volume fraction.[70] (b) Molecular weight dependence of the PNC viscosity adjusted by the self-diffusion coefficient.

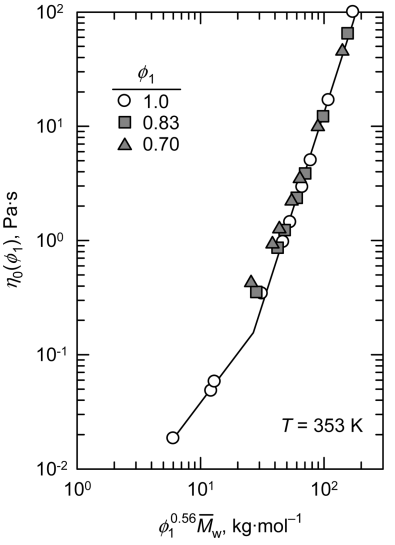

Figure 9. Effect of volume fraction and weight-average molecular weight of PDMS on the zero-shear-rate viscosity of the polysilicate-filled nanocomposite in the regime $M > M_c$.

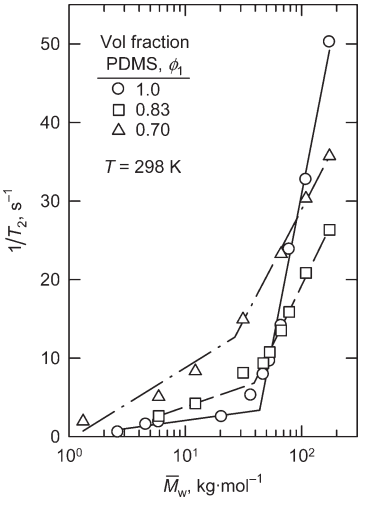

Figure 10. Effect of polysilicate nanoparticle on the molecular weight dependence of the NMR spin−spin relaxation time of PDMS at 298 K.

relative viscosity data at 353 K collapsing into the same line for the unfilled polymer ($\phi_1 = 1$) when plotted versus $\phi_1^{0.56}\bar{M}_w$. Taking into account the slope of the line (3.5)

$$\frac{\eta_0(\phi_1)}{\eta_0(1)} \sim \phi_1^{2}\bar{M}_w^{3.5} \quad \begin{matrix} M > M_c, \\ \phi_1 \geq 0.7 \end{matrix} \tag{14}$$

The deviation apparent in the vicinity of M_c was attributed to a crossover to a different mechanism (reinforcement) imparted by the nanoparticle in the regime below M_c, and which could be minimized to some extent by taking to account the friction factor.

NMR Relaxation Measurements. The characterization of the NMR T_2 spin−spin relaxation times for the polymers and PNCs were also completed at 298 and 353 K. The results at 298 K are shown in Figure 10 as the relaxation rate constant $1/T_2$ as a function of log $\bar{M}_w$.

The pure PDMS data showed a characteristic break at a molecular weight of ~44 kg·mol^{-1} where the effects from entanglements become an important relaxation mechanism. This value was significantly greater than values from the viscosity measurements and a previous NMR study,[39] and unlike viscosity may have been influenced by polydispersity effects. The time and length scales of the NMR experiments are considerably shorter than viscosity measurements and the relative contributions from diffusion and rotation/reptation motion to the NMR relaxation rates determine their values. Above M_c, the reduced diffusion and hindered rotation lead to a rapid decrease in T_2. Since the R2 nanoparticle protons have relaxation times much shorter than that of the polymer protons, the relaxation times measured in the CPMG experiment[49,50] relate to the mobility of the polymer component of the PNCs and not the nanoparticles per se. This is because the strong dipolar coupling in the solid state is not refocused by a conventional 180° RF pulse as used in this sequence. Hence, beyond the first echo there is no solid-state

signal. From Figure 10, it was quite clear that below M_c the nanoparticles reduced the local mobility as seen from the T_2 data and in comparing the two volume fractions the reduction in mobility was enhanced by increasing the concentration of nanoparticles as expected, which was consistent with the viscosity results in Figure 3. However, above M_c the nanoparticle content was less effective at restricting the mobility and there was a crossover whereby the PNCs were more mobile than the pure polymer. In addition, the dependence of polymer $\overline{M}_w$ on $1/T_2$ decreased as the concentration of nanoparticles increased in agreement with the viscosity data. These effects have been discussed in some detail before[8,9] and are a balance of changes in free volume, reduced entanglements due to adsorption and possibly a degree of flocculation. However, the mechanism for flocculation is unclear because, in this case, the polymer adsorbs onto the nanoparticle and the PNCs appear optically clear and stable.

In contrast with the viscosity results, the M_c based on T_2 relaxation times for the PNCs with $\phi_1 = 0.83$ shifted to a lower value of $\sim$39 kg·mol^{-1} and fell further for $\phi_1 = 0.70$ to $\sim$27 kg·mol^{-1}, and a model based on chain collapse upon adsorption will increase in effectiveness as more surface area is available.

The examination of the results at 353 K revealed similar trends except the PNCs expectedly became much more mobile and restrictions on the polymer mobility by the nanoparticles were significantly reduced. This was especially evident above 80 kg·mol^{-1} which is well within the entanglement regime.

Conclusions

Hard spherical polysilicate nanoparticles up to 0.30 volume fraction were used to impact the dynamics of PDMS polymers spanning both unentangled and entangled molecular weight regimes. Below the polymer M_c, the incorporation of nanoparticles increased η_0 relative to the polymer matrix consistent with the reinforcement mechanism observed in composites using traditional fillers of much larger particle sizes. Above M_c, η_0 decreased with increasing nanoparticle loadings up to a volume fraction of 0.30. The reduction in η_0 was proposed to be primarily due to the dilution of the entanglement density of polymer chains as evidenced by a shift to higher M_c that was a function of the volume fraction of polymer chains, ${\phi_1}^{-0.56}$, and an increase in the translational motion manifested through D_s. Above M_c, the PNC η_0 scaled as $\phi^2{\overline{M}_w}^{3.5}$. In another experimental time scale, NMR T_2 spin−spin relaxation measurements revealed that the nanoparticles reduced the polymer mobility to molecular weights that exceeded the viscosity-based M_c. An increase in polymer mobility due to the nanoparticles became evident only when $M > 2M_c$. In contrast to the viscosity results, the transition to a stronger $\overline{M}_w$ dependence by $1/T_2$ shifted to lower molecular weights with increasing nanoparticle concentration.

Acknowledgments

R.G.S. and G.V.G. acknowledge A. L. Tanke and L. L. Myers for material characterization, and T.C. thanks Y. Espidel for PGSE−NMR data.

References and Notes

(1) Nielsen, L. E.; Landel, R. F. *Mechanical Properties of Polymers and Composites*, 2nd ed.; Marcel Dekker: New York, 1994.
(2) Chong, J. S. Ph.D. Thesis. University of Utah, 1962.
(3) Farris, R. J. *Trans. Soc. Rheol.* **1968**, *12*, 281–301.
(4) Chong, J. S.; Christiansen, E. B.; Baer, A. D. *J. Appl. Polym. Sci.* **1971**, *15*, 2007–2021.
(5) *Handbook of Plasticizers*; Wypych, G., Ed.; ChemTec Publishing: Toronto, Canada, 2004.
(6) Giannelis, E. P. *Adv. Mater.* **1996**, *8*, 29–35.
(7) Roberts, C. H. Ph.D. Thesis. University of Bristol: Bristol, U.K., Sep. 2000.
(8) Roberts, C.; Cosgrove, T.; Schmidt, R. G.; Gordon, G. V. *Macromolecules* **2001**, *34*, 538–543.
(9) Cosgrove, T.; Roberts, C.; Choi, Y.; Schmidt, R. G.; Gordon, G. V.; Goodwin, A. J.; Kretschmer, A. *Langmuir* **2002**, *18*, 10075–10079.
(10) Cosgrove, T.; Roberts, C.; Garasanin, T.; Schmidt, R. G.; Gordon, G. V. *Langmuir* **2002**, *18*, 10080–10085.
(11) Roberts, C.; Cosgrove, T.; Schmidt, R. G.; Gordon, G. V.; Goodwin., A. J.; Kretschmer, A. In *Synthesis and Properties of Silicones and Silicone-Modified Materials*; Clarson, S. J., Fitzgerald, J. J., Owen, M. J., Smith, S. D., Van Dyke, M. E., Eds.; ACS Symposium Series 838; American Chemical Society: Washington, DC, 2003; pp 181−192.
(12) Benton, N. J. Ph.D. Thesis. University of Bristol: Bristol, U.K., Sep. 2004.
(13) Schmidt, R. G.; Gordon, G. V.; Dreiss, C. A.; Cosgrove, T.; Krukonis, V. J.; Williams, K.; Wetmore, P. M. *Macromolecules* DOI: 10.121/ma1004919.
(14) Mackay, M. E.; Dao, T. T.; Tuteja, A.; Ho, D. L.; Van Horn, B.; Kim, H.-C.; Hawker, C. *J. Nat. Mater.* **2003**, *2*, 762–766.
(15) Tuteja, A.; Mackay, M. E.; Hawker, C. J.; Van Horn, B. *Macromolecules* **2005**, *38*, 8000–8011.
(16) Tuteja, A.; Duxbury, P. M.; Mackay, M. E. *Macromolecules* **2007**, *40*, 9427–9434.
(17) Tuteja, A.; Mackay, M. E.; Narayanan, S.; Asokan, S.; Wong, M. S. *Nano Lett.* **2007**, *7*, 1276–1281.
(18) Kopesky, E. T.; Haddad, T. S.; Cohen, R. E.; McKinley, G. H. *Macromolecules* **2004**, *37*, 8992–9004.
(19) Jordan, J.; Jacob, K. I.; Tannenbaum, R.; Sharaf, M. A.; Jasiuk, I. *Mat. Sci. Eng.* **2005**, *393*, 1–11.
(20) Brochard Wyart, F.; de Gennes, P. G. *Eur. Phys. J. E* **2000**, *1*, 93–97.
(21) Smith, G. D.; Bedrov, D.; Li, L.; Byutner, O. *J. Chem. Phys.* **2002**, *117*, 9478–9489.
(22) Kairn, T.; Davis, P. J.; Ivanov, I.; Bhattacharya, S. N. *J. Chem. Phys.* **2005**, *123* (19); Art. No. 194905.
(23) Ganesan, V.; Pryamitsyn, V.; Surve, M.; Narayanan, B. *J. Chem. Phys.* **2006**, *124* (22); Art. No. 221102.
(24) Pryamitsyn, V.; Ganesan, V. *J. Rheol.* **2006**, *50*, 655–683.
(25) Sen, S.; Thomin, J. D.; Kumar, S. K.; Keblinksi, P. *Macromolecules* **2007**, *40*, 4059–4067.
(26) Fetters, L. J.; Lohse, D. J.; Milner, S. T.; Graessley, W. W. *Macromolecules* **1999**, *32*, 6847–6851.
(27) Rouse, P. J. *J. Chem. Phys.* **1953**, *21*, 1272–1280.
(28) Bueche, F. *J. Chem. Phys.* **1952**, *20*, 1959–1964.
(29) Doi, M.; Edwards, S. F. *The Theory of Polymer Dynamics*; Clarendon Press: Oxford, U.K., 1986.
(30) de Gennes, P. G. *J. Chem. Phys.* **1971**, *55*, 572–579.
(31) Colby, R. H.; Fetters, L. J.; Graessley, W. W. *Macromolecules* **1987**, *20*, 2226–2237.
(32) Fetters, L. J.; Graessley, W. W.; Kiss, A. *Macromolecules* **1991**, *24*, 3136–3141.
(33) Doi, M. *J. Polym. Sci., Polym. Phys. Ed.* **1983**, *21*, 667–684.
(34) Milner, S. T.; McLeish, T. C. B. *Phys. Rev. Let.* **1988**, *81*, 725–496.
(35) Graessley, W. W. *Adv. Polym. Sci.* **1982**, *47*, 67–117.
(36) Brereton, M. G. *Macromolecules* **1989**, *22*, 3667–3674.
(37) Brereton, M. G. *Macromolecules* **1990**, *23*, 1119–1131.
(38) Brereton, M. G.; Ward, I. M.; Boden, N.; Wright, P. *Macromolecules* **1991**, *24*, 2068–2074.
(39) Cosgrove, T.; Griffiths, P. C.; Hollingshurst, J.; Richards, R. D. C.; Semlyen, J. A. *Macromolecules* **1992**, *25*, 6761–6764.
(40) Friedman, E. M.; Porter, R. S. *Trans. Soc. Rheol.* **1975**, *19*, 493–508.
(41) Li, G.; Wang, L.; Ni, H.; Pittman, C. U., Jr. *J. Inorg. Organomet. Polym.* **2002**, *11*, 123–154.
(42) Merrill, D. F. *Adhes. Age* **1979**, *22* (3), 39–41.
(43) *Handbook of Pressure-Sensitive Adhesive Technology*; Satas, D., Ed.; Van Nostrand Reinhold: New York, 1982: Chapters 15 and 18.
(44) Daudt, W.; Tyler, L. U.S. Patent 2,676,182, 1954.
(45) McHugh, M. A.; Krukonis, V. J. *Supercritical Fluid Extraction: Principles and Practices*, 2nd ed.; Butterworth-Heinemann: Boston, MA, 1994; Chapter 9.
(46) Fetters, L. J.; Lohse, D. J.; Richter, D.; Whitten, T. A.; Zirkel, A. *Macromolecules* **1994**, *27*, 4639–4647.

(47) Orrah, D. J.; Semlyen, J. A.; Ross-Murphy, S. B. *Polymer* **1988**, *29*, 1452–1454.
(48) Langley, N. R.; Mbah, G. C.; Freeman, H. A.; Huang, H.-H.; Siochi, E. J.; Ward, T. C.; Wilkes, G. *J. Colloid Interface Sci*. **1991**, *143*, 309–317.
(49) Carr, H. Y.; Purcell, E. M. *Phys. Rev*. **1954**, *94*, 630–638.
(50) Meiboom, S.; Gill, D. *Rev. Sci. Instrum*. **1958**, *29*, 688–691.
(51) Provencher, S. W. *J. Chem. Phys*. **1976**, *64*, 2772–2777.
(52) McCall, D. W.; Anderson, E. W. *J. Chem. Phys*. **1961**, *34*, 804–808.
(53) Barlow, A. J.; Harrison, G.; Lamb, J. *Proc. R. Soc. London* **1964**, *A282*, 228–251.
(54) Batchelor, G. K. *J. Fluid Mech*. **1977**, *83*, 97–117.
(55) Einstein, A. *Ann. Phys*. **1906**, *19*, 289–306.
(56) Einstein, A. *Ann. Phys*. **1911**, *34*, 591–592.
(57) Mooney, M. *J. Colloid Sci*. **1951**, *6*, 162–170.
(58) Meeker, S. P.; Poon, W. C. K.; Pusey, P. N. *Phys. Rev. E* **1997**, *55*, 5718–5722.
(59) Batchelor, G. K. *J. Fluid Mech*. **1976**, *74*, 1–29.
(60) Bueche, F. *J. Appl. Phys*. **1953**, *24*, 423–427.
(61) Bueche, F. *J. Appl. Phys*. **1955**, *26*, 738–749.
(62) Schmidt, R. G.; Badour, L. R.; Gordon, G. V. In *Synthesis and Properties of Silicones and Silicone-Modified Materials*; Clarson, S. J., Fitzgerald, J. J., Owen, M. J., Smith, S. D., Van Dyke, M. E., Eds.; ACS Symposium Series 838; American Chemical Society: Washington, DC, 2003; pp 170−180.
(63) Ferry, J. D. *Viscoelastic Properties of Polymers*, 3rd ed.; Wiley: New York, 1980.
(64) Colby, R. H.; Rubinstein, M. *Macromolecules* **1990**, *23*, 2753–2757.
(65) Colby, R. H.; Rubinstein, M. *Polymer Physics*; Oxford University Press: Oxford, U.K., 2003; p 369.
(66) de Gennes, P. G. *Macromolecules* **1976**, *9*, 587−593; 594−598.
(67) Milner, S. T. *Macromolecules* **2005**, *38*, 4929–4939.
(68) Graessley, W. W.; Edwards, S. F. *Polymer* **1981**, *22*, 1329–1334.
(69) Marin, G.; Menezes, E.; Raju, V. R.; Graessley, W. W. *Rheol. Acta* **1980**, *19*, 462–476.
(70) Espidel, Y.; Muangapil, S.; Cosgrove, T.; Schmidt, R. G. Manuscript in preparation.
(71) Appel, G.; Fleischer, G. *Macromolecules* **1993**, *26*, 5520–5525.